ACS OMEGA

Open Access

http://pubs.acs.org/journal/acsodf

Article

Detection of Ultraviolet Light by Graphene Oxide Derived from Epitaxial Graphene on SiC and Graphite

Md. Zakir Hossain* and Ogawa Kosei

Cite This: *ACS Omega* 2024, 9, 32942−32948

Read Online

ACCESS | Metrics & More | Article Recommendations | Supporting Information

ABSTRACT: Because of their tunable band gap, flexibility, and high surface-to-volume ratio, two-dimensional materials have appeared as the most promising materials for ultraviolet (UV) light sensors. Here, we report the detection of UV light by oxidized epitaxial graphene (EG) formed on the Si-face of the SiC substrate and graphene oxide (GO) produced by Hummer oxidation of graphite. Both epitaxial graphene oxide (EGO) and GO were characterized by Raman and X-ray photoelectron spectroscopy, and the devices were made simply by placing two parallel copper electrodes onto the graphene oxide layers. Irradiation of UV light onto the graphene oxides was realized by the real-time current measurements between two electrodes at a fixed bias of 1 V. The sudden upward jump of the current (Ids) upon UV light irradiation was observed in both EGO- and GO-based devices, which were returned to the original value, while the UV source was turned OFF. The photocurrent (I_{ph}), the magnitude of the current jump by the UV irradiation, for EGO, was estimated at 8 mA with a channel distance of 2 mm and UV power of 80 mW/cm^2. The I_{ph}linearly increases with UV power. In the case of GO, $I_{ph}$was estimated at 0.2 nA with a similar setup. The photoresponse time and responsivity for EGO are ∼11 s and 5.6 A/W, respectively, which are higher than those of GO. The quantum efficiencies (η) for EGO and GO are calculated as 1907 and 2.3 × 10^{-6} %, respectively, with an incident power of UV light at 9 mW/cm^{-2}. Because of the advantages of the EG on SiC concerning the stability and wafer scale growth, the present study is expected to lead the development of lab-on-chip-based ultrasensitive UV sensors.

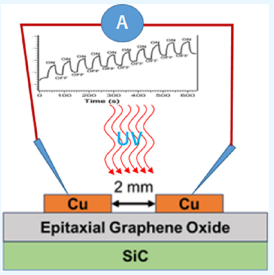

1. INTRODUCTION

Ultraviolet (UV) radiation, electromagnetic radiation within the wavelength range of 10−400 nm, is abundantly present in sunlight. It can also be generated by various artificial light sources for different purposes.[1,2] Although UV light is generally used as an important optical source for many applications such as semiconductor lithography, polymer curing, sterilization, and disinfection of medical equipment and everyday supplies, bioanalysis and cell imaging, light therapy, and beauty care and antiaging treatment, it can also adversely affect all living things.[1−4] In humans, overexposure to UV radiation is associated with the development of various skin-related diseases including erythema, pigment darkening, sunburn, skin cancers, and cancer of the cornea and conjunctiva.[5,6] To prevent harmful effects, frequent monitoring and instantaneous warning of personal UV exposure are necessary. A UV light sensor is based on the response of the material's electrical properties, such as conductivity and resistance by the irradiation of UV light.

So far, various large band gap semiconductor materials have been explored to manufacture ultraviolet sensors, such as type III-nitrides and II−VI, III−VI, and IV−VI compounds.[7,8] Semiconductor materials have great potential to be used as photoelectric sensors because they offer the opportunity to tune their band gap in the UV region of the electromagnetic spectrum. Among the different semiconductors, ZnO, TiO_2, Zn_2SnO_4, $ZnGa_2O_4$, ZnMgO, Zn_2GeO_4, SnO, SnO_2, NiO, Nb_2O_5, $K_2Nb_8O_{21}$, Ta_2O_5, and Ga_2O_3 have been widely studied because of their abundant reserves, excellent stability, and environmentally beneficial properties.[7,8] Other wide band gap materials such as metal nitrides, metal sulfides, metal selenides, carbon-based materials, and 2D analogues of graphene, such as phosphorene, have been investigated.[9−18] Recently, it has been found theoretically that metal oxide semiconductors binding with two-dimensional (2D) materials show higher photoresponse than their bulk because of their large specific surface area and incomparable thinness.[14−16] Since the invention of graphene in 2004, many studies involving UV photodetectors have been reported based on two-dimensional (2D) materials.[19,20]

Graphene, considered the material for the future, is a 2D zero band gap material that can readily be obtained by exfoliation of graphite, chemical vapor deposition on the metal substrate, or epitaxial growth on SiC.[19−21] Because of its excellent optical, electrical, and mechanical properties, graphene has appeared as the most promising material in materials science, micro/nanoprocessing, energy, and different types of sensors, such as graphene capacitors, nanopower

Received: April 23, 2024
Revised: June 28, 2024
Accepted: July 9, 2024
Published: July 18, 2024

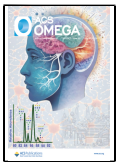

generators, and superconductors.[20,22,23] Graphene has been extensively studied for the development of various types of graphene field-effect transistor-based gas sensors and biochemical sensors.[24] The zero band gap and one atom thickness make the graphene almost transparent and found to absorb a (pa = 2.3%) little fraction of incident white light.[25] Hence, the pristine graphene cannot be utilized as a light sensor.

In contrast to pristine graphene, graphene oxide derived from graphite or epitaxial graphene exhibits a significant band gap.[26−30] The band gap of graphene oxide varies with the extent of oxidation of graphene carbon atoms. Hence, the band gap of graphene oxide is tunable, which makes it a promising material for the light sensor.[28,29] The band gap in GO is ∼2.2 eV, and for reduced GO (RGO), the band gap can vary from ∼1.00 to 1.69 eV depending on the degree of reduction.[28,29] To date, some studies involving UV detection have been reported on GO- or RGO-based sensors. Wang et al. reported a low-cost, high-performance UV sensor compatible with flexible electronics from an azide-shaped ZnO film modified with reduced graphene oxide (RGO) on a PDMS substrate and showed a significant increase in the on/off ratio and photoresponse current by introducing an appropriate weight ratio of RGO.[31] Chitara et al. also reported UV response in devices with several layers of RGO films on ITO/glass substrates.[32] Abusultan et al. have reported an oxide (GO)-based paper UV sensor and demonstrated its capability and feasibility of commercial utilization.[33]

To date, most of the reported studies have focused on thin GO or RGO films.[31−33] Indeed, fabrication of a sensor consisting of a monolayer graphene between the electrodes in lateral configuration is a difficult and expensive task since it requires high-end nanoscale manipulation techniques. However, a single layer of graphene oxide can be easily obtained by the control oxidation of EG on SiC.[27] To the best of our knowledge, no studies have been reported on EG on SiC-based UV sensors. Indeed, instead of graphite-derived graphene oxide, epitaxial graphene oxide has the advantage of being produced on a wafer scale and with enhanced stability. Recently, we have developed a control method of oxidation of EG on SiC, resulting in one to three layers of graphene oxide supported onto the SiC substrate.[27] Thus produced EGO on a SiC substrate can readily be used in UV sensing devices without any complex transfer process or treatments. The band gap of such EGO on SiC is estimated to be 0.4 eV.[27] Hence, the epitaxial EGO on SiC is expected to show an excellent response to ultraviolet light, leading to the development of an integrated array of UV sensors on a wafer scale. Here, we investigated the UV response of UV light on EGO on SiC and compared the results with those of a thin film of GO.

2. MATERIALS AND METHODS

The most common and powerful method for preparing graphene oxide from graphite is the Hummers method and the modified Hummers method of oxidation.[34] In the Hummers method, a mixture of $NaNO_3$, $KMnO_4$, and H_2SO_4 was used as the oxidizing agent. For oxidation of graphite, 0.6 g of graphite, 0.1 g of $NaNO_3$, and 1.8 g of $KMnO_4$ were added to 20 mL of concentrated H_2SO_4 with constant stirring in an ice bath for ∼1 h. At this time, the solution turned dark green. The mixture was then stirred for 3 h while being maintained at a constant temperature (35 °C). At this stage, the color of the solution changed from dark green to brown, and then, 10 mL of hydrogen peroxide water was added until the color of the solution changed from brown to yellow. The GO mixture was stirred in a hot water bath at 90−100 °C for 2 h, which turned the solution black. The resulting black graphene oxide solution was centrifuged to separate the graphene oxide layer from the unoxidized graphite. The supernatant of the GO solution was collected, and a few drops of the GO solution were carefully placed on a clean glass slide. The glass slide was then allowed to dry under ambient conditions. When the water of the GO solution was dried up, a thin film of GO (∼1 μm) was obtained on a glass slide by heating it in an oven below 100 C.

EG on SiC was prepared by annealing a piece (1 cm × 2 cm cut) of the 6H-SiC(0001) sample at 1350 °C for five to six cycles of 1 min in a UHV chamber with a maximum pressure of ∼5.0×10^{-9} Torr. Thus, the prepared EG on the Si-face of the SiC substrate usually contains one to three layers of graphene.[35] The EG grown in UHV was oxidized *ex situ* using Hummer's oxidizing agents (mixture of $NaNO_3$, $KMnO_4$, and H_2SO_4). In the "drop-cast" procedure, a few drops of Hummer solution were carefully placed onto the EG on the SiC surface.[34] The sample was then placed on a hot plate and heated to ∼60 C for faster oxidation. After oxidation, the sample was cleaned by DI water and H_2O_2 repeatedly. Thus, one to three layers of EGO on SiC could be obtained. A typical scanning tunneling microscope (STM) image of EGO on SiC is shown in the Supporting Information.

The EG on SiC, EGO, and GO was characterized by Raman and X-ray photoelectron spectroscopy (XPS). Raman measurements were carried out by a Nicolet Almega XR Raman spectroscope with a 532 nm laser. XPS was carried out by an AXIS-NOVA. The X-ray target is Al ($h\nu$ = 1486.6 eV).

The UV response on the resistive current of the EGO on SiC and GO was monitored by making simple devices consisting of two copper electrodes 2 and 8 mm apart by attaching copper tape, as schematically shown in Figure 1. Since the two copper electrodes were in ohmic contact with the graphene oxides supported on an insulating substrate, the device can be categorized as a photoconductive detector.[36] The entire detection experiment was performed in complete

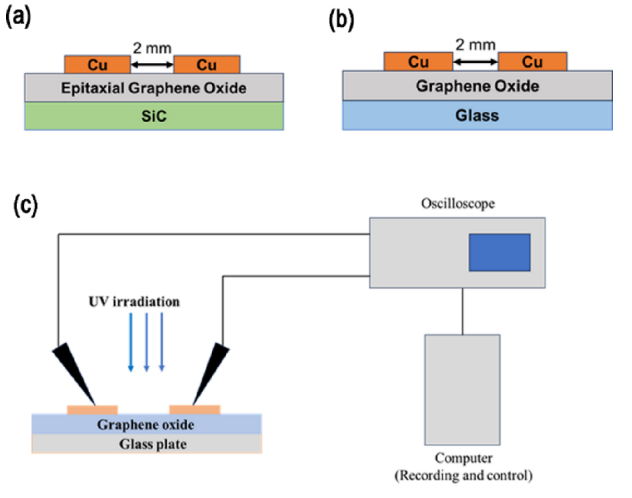

Figure 1. Schematic of the devices used for the measurement of UV response on the resistive current of (a) epitaxial graphene oxide (EGO) on a SiC substrate and (b) graphene oxide (GO) on glass. (c) Setup for real-time two-terminal measurements of resistive current with UV light ON and OFF states.

https://doi.org/10.1021/acsomega.4c03882
ACS Omega 2024, 9, 32942−32948

darkness to ensure that it was not affected by ambient light to the greatest extent. An AS ONE LUV-16 instrument was used as the ultraviolet light (365 nm) source in the test. Two-probe surface conductivity measurement was performed using a homemade probing system with W probes and a LabVIEW system (National Instruments). A Keysight 4155B semiconductor parameter analyzer was used for monitoring the real-time current while switching the UV source ON and OFF states periodically. The drain voltage was maintained at 1 V, while the source terminal was grounded.

3. RESULTS AND DISCUSSION

3.1. Characterization of EGO and GO. The most reliable and commonly used technique for the characterization of graphene and its oxide derivatives is Raman spectroscopy. For the pristine graphene, two major characteristics bands, 2D (~2700 cm^{-1}) and G (~1600 cm^{-1}), are observed. Figure 2

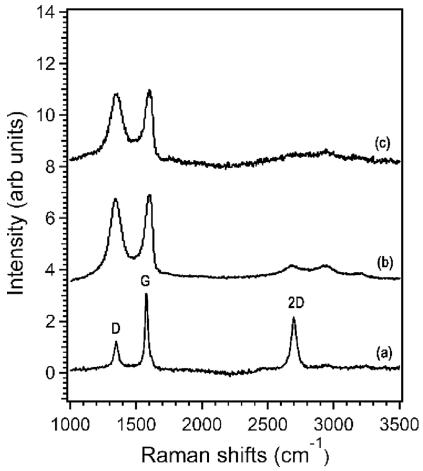

Figure 2. Raman spectra of (a) pristine epitaxial graphene (EG) on SiC, (b) oxidized EG on SiC, and (c) graphene oxide (GO) obtained from the oxidation of graphite.

shows the typical Raman spectra of pristine EG on SiC, EGO on SiC, and GO. The G band is ascribed to the in-plane vibration of sp^2 carbon atoms, which is a doubly degenerate phonon mode (E_{2g} symmetry) at the Brillouin zone center.[37] The 2D band is a two-phonon process, which is allowed only for a perfect lattice of graphene.[37] The small D peak at 1380 cm^{-1} is a defect-induced band, which appears in the case of clean graphene on SiC due to the interaction of graphene with the substrate.[37] The graphene oxide possesses a variety of oxygen moieties such as epoxy, ether, carboxylic, hydroxyl, and carbonyl groups at the edge and on the basal plane of the GO sheet, i.e., the continuity of the hexagonal lattice is broken. Hence, the oxidation of graphene induces a decrease in the intensity of the 2D band and increases the D band, as observed in the Raman spectra of EGO on SiC and GO (Figure 2). The further confirmation of oxidation of graphene was confirmed by XPS measurements. The high-resolution C 1s spectra of EGO and GO (Figure 3a) show the oxidized C 1s peaks around 286 eV. Though the oxidized graphene contains varieties of O-containing functional groups such as epoxy, ether, carbonyl, etc., the deconvoluted individual peaks are not observed. The lower energy peak around 284.7 eV is ascribed to C 1s of graphene carbon atoms. To see the effect of UV light on the conductivity of oxidized graphene, graphene oxide

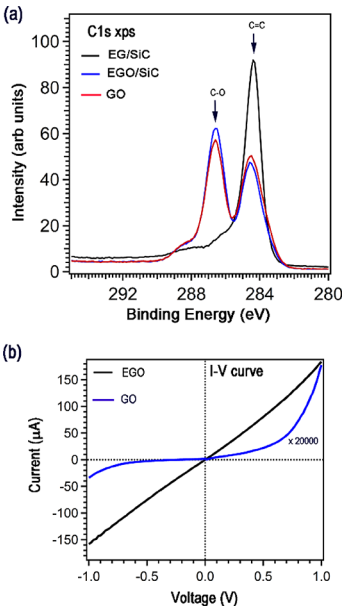

Figure 3. (a) High-resolution C 1s spectra of pristine EG on SiC, oxidized EG on SiC, and GO obtained from the oxidation of graphite. The C 1s peaks arise from the graphene carbon, and oxidized carbon is indicated as C═C and C−O. (b) Current (I) vs voltage (V) curves for EGO on SiC and GO on glass-based devices.

must be conductive. The conductivity of oxidized graphene was investigated by two terminal I (current)−V (voltage) measurements. Figure 3b shows the typical I−V curves of EGO on SiC and the GO film on glass. The results indicate that current passes through EGO on SiC and GO on glass. The large difference in the I−V curves of EGO and GO is due to the different extent of oxidation of graphene, which makes the band gap differences. The extent of oxidation of EGO obtained by a mild drop-cast procedure is much lower than that of GO obtained by vigorous Hummer's oxidation.[27] Although the electrodes are similar in both devices, the lower current in GO-based devices is due to the large band gap and higher resistivity of the GO film. Note that the resistivity of the SiC substrate is very high, and it does not conduct any current under the present setup. Hence, EGO and GO can be used to see the effects of UV light on their conductivity by two terminal measurements.

3.2. Effect of UV Irradiation on the Conductivity of EGO and GO-Based Devices. The UV response of a material can be realized by the photoconductive effect of the material. The positive photoconductive effect arises from the excitation of additional carriers into the conduction states or any other midgap states, which can ultimately modulate the conductivity of the material that acts as the channel of the carriers.[38−41] These excited additional carriers can be converted into the current by applying an external bias through symmetrical contacts onto the channel materials through which the additional carriers are dumped. Hence, for the detection of the UV response on the conductivity of EGO, the two terminal current measurements were done in real time by connecting the two tungsten probes onto the two copper electrodes (as shown in Figure 1) while the device was intermittently irradiated with UV light for a certain time. Figure 4a shows the real-time current (Ids) data of the EGO on a SiC-based device while the UV source is turned "ON" and "OFF" periodically. When the UV source is turned ON, a sudden jump in the Ids

https://doi.org/10.1021/acsomega.4c03882
ACS Omega 2024, 9, 32942−32948

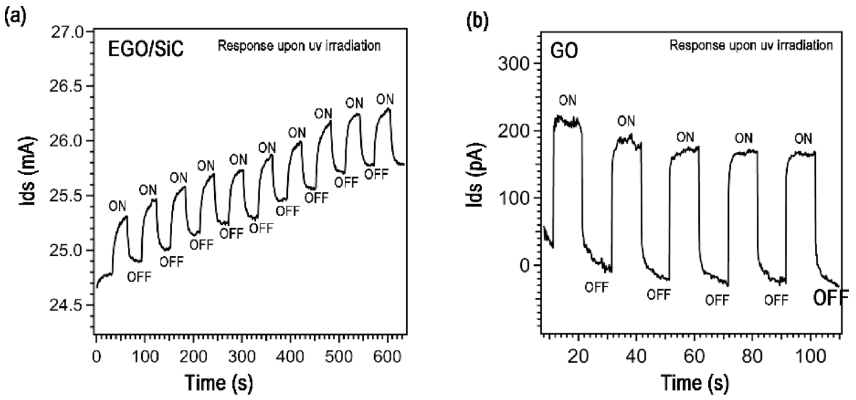

Figure 4. Real-time current (Ids) values upon sequential irradiation of UV lights on (a) EGO on SiC and (b) GO on glass-based devices.

value between the two electrodes is observed. When the UV source is turned OFF, the Ids value immediately returns to the initial value. The periodic changes of the current in response to UV light confirm the reproducibility of the UV-induced photocurrent for the EGO on SiC-based devices. With the UV source setting at 10 cm above the EGO on the SiC surface, the jump of the Ids value to ∼8 mA was observed. The jump of the Ids value upon irradiation of UV light relates to the photoexcitation of electrons leading to the generation of electron−hole pairs in EGO.[39,40] The photoexcitation process may involve both the conduction band states and defect-induced midgap states, where the electrons can temporarily be trapped.[40] Note that these defect-induced states in GO are expected to be much higher than those of EGO, which is negligible in the case of pristine EG on SiC.

It can be seen in Figure 4a that the initial Ids values (dark current) gradually increase with the increase in the number of irradiation cycles. The exact reason behind this gradual increase in the dark current (Figure 4a) is not clearly understood at this stage. This phenomenon can be derived from the electrode/photoconductor ohmic contact, photoconductor/substrate interface, or bulk properties of the conducting material, i.e., graphene oxide.[41] Apparently, the electrode/material contact in the present study is similar for EGO- and GO-based devices, but the dark current gradually increases only for EGO-based devices. Hence, the gradual increment of dark current may not come from the effect of electrode/material contact. The phenomenon may also not relate to the photoconductor/substrate interface because the GO thin film on the SiC substrate gives similar results (Figure S1a in the Supporting Information) to that on the glass substrate (Figure 4b). Hence, the gradual increases in dark current upon periodic exposure to UV light most likely arise from the intrinsic properties of EGO. Indeed, different types of currents such as diffusion current, trap-assisted tunneling current, generation-recombination current, surface leakage current, etc. can contribute to the dark current of a photoconductive device.[41] Similar to the photocurrent, the dark current may be generated by the thermal excitation of the carriers to the conduction band or defect states related to the lattice defect in graphene or oxygen impurities. Since the main difference between the EGO- and GO-based devices in the present study is the band gaps of the photoconductor materials, i.e., the extent of oxidation, the observed phenomenon may arise from the thermal excitation of the carrier into the conduction band. Most likely, the sequential irradiation of UV light causes the gradual increase in temperature of the graphene oxide channel, which induces the excitation of carriers into the conduction or defect states in the case of EGO-based devices because of the low energy band gap (0.4 eV) of EGO.

Similar to EGO on SiC-based devices, GO-based devices also exhibit UV responsivity with a jump of Ids values upon irradiation of the device with UV light, as shown in Figure 4b. In the case of GO-based devices, the current jump was estimated at about 0.2 nA with the UV source set at a distance of 10 cm. The lower Ids value compared to the EGO-based device may relate to the aggressive oxidation of graphite by the Hummers method, resulting in the higher resistivity, which is realized in the *I*−*V* data shown in Figure 3b. To see that the photoresponse arises from the graphene oxide, several blank tests with the light source and materials were performed. No changes in the Ids value were observed when the EGO on SiC and GO film on glass were irradiated with white light, but they readily responded to UV light, as shown in Figure 5a,b. In addition, pristine EGs on SiC and SiC substrate itself do not show any responsivity upon UV light irradiation under a similar setup to that of EGO- and GO-based devices (Figure S1b in the Supporting Information). Thus, blank experiments confirm that the UV response arises purely from the EGO on

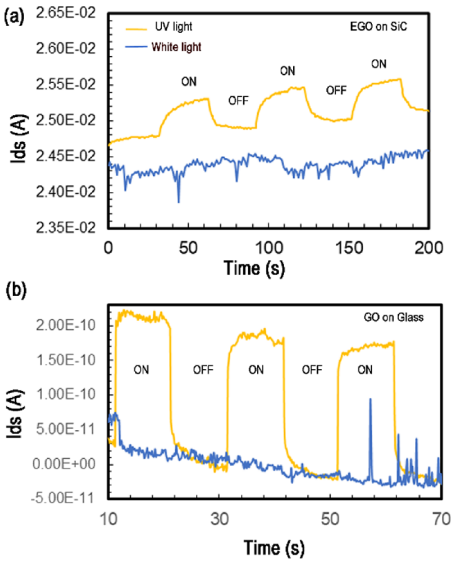

Figure 5. Effects of UV and white light on (a) EGO on SiC and (b) GO-based devices.

https://doi.org/10.1021/acsomega.4c03882
ACS Omega 2024, 9, 32942−32948

SiC and the GO layers on glass. It should also be noted that the photoinduced jump of the Ids value in the case of a GO-based device was only observed when the two electrodes were attached on top of the thin GO film, as shown in Figure 1, i.e., the GO layers exposed to UV light are in direct ohmic contact with the metal (Cu) electrodes. No photoinduced current is observed when the electrodes are placed at the back of the GO film. This phenomenon may depend on the thickness of the film, which has yet to be explored.

The jump of the Ids value upon UV light irradiation is normally termed photocurrent (I_{ph}). It is well known that the photocurrent of a material depends on the power (i.e., intensity) of the UV irradiation. The $I_{ph}$of a photodetector device is expressed by $I_{ph} = I_{uv} - I_{dark}$, where I_{uv} is the current under UV irradiation and I_{dark} is the current under a dark environment. The dependence of I_{ph}on the intensity of the UV light has been investigated by adjusting the intensity of the UV light by changing the distance between the device and the UV light. The irradiation output of the UV light source used in this experiment is 4000 mW/cm^2. The area exposed to UV light was measured to be 50 cm^2 when irradiated with UV light at a distance of 10 cm. We estimated the UV intensity based on this value and did the measurements at various distances. Figure 6a,b shows the real-time Ids values at different

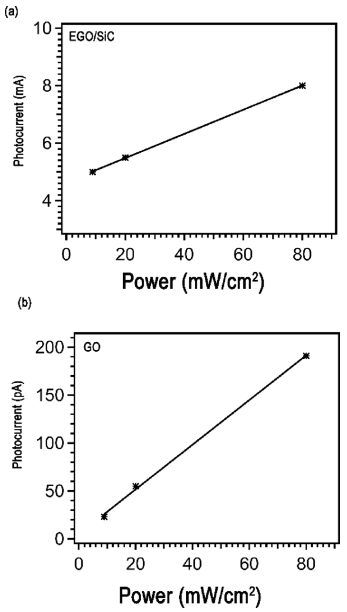

Figure 6. Dependences of photocurrents with the power of UV lights of (a) EGO on SiC and (b) GO on glass-based devices.

intensities of UV lights irradiated onto EGO on SiC and GO on glass-based devices. Measurements were taken at distances of ∼10, 20, and 30 cm from the UV source to the device. In the case of GO (Figure 6b), the photocurrent (I_{ph}) increases sharply with UV intensities compared to that of EGO on SiC-based devices. It should be noted that in addition to the intrinsic properties of channel materials and power of irradiation, the I_{ph}also depends on the geometry of the device, i.e., the length (L) and width (W) of the channel as I_{ph} is proportional to W/L. With decreasing the length of the GO channel, the I_{ph}can be enhanced. A simple channel length-dependent experimental data set is shown in Figure S1 in the Supporting Information.

3.3. Photoresponsivity and Response Time of the Devices. In addition to the aforementioned photocurrent I_{ph}, two other parameters are also evaluated for the characterization of a UV detector: the photoresponsivity (R) and response times. Photoresponsivity is expressed by the following formula, $R = I_{ph}/(P_{in} \times S)$, where P_{in} is the UV power per unit area (mW/cm^2), and S is the effective area of the device. The effective device areas were calculated as 0.1 cm^2 for EGO and 0.4 cm^2 for GO when the channel distance was 2 mm. The response time includes two terms, the rising time (τ_r) and falling time (τ_f), which are defined as the time required for increasing the Ids values from 10 to 90% and decreasing the Ids values from 90 to 10% of the photocurrent, respectively (as shown in Figure S2 in the Supporting Information). The estimated parameters at different UV intensities for both EGO on SiC and GO on glass-based devices are listed in Table 1.

The response times for reduced graphene oxides estimated from three terminal measurements were reported to be 2 and 100 s, while the responsivities were reported to be 4 and 0.12 A/W.[39,40] For a two-terminal measurement with reduced graphene oxide nanosheets, the response time and responsivity are reported as 1 s and 3.74 A/W, respectively.[18] Note that the response (τ_r) and falling (τ_f) times of a photodetector depend on many factors including the intrinsic properties of the photoconductor, light wavelength, nature and concentration of defects, temperature, electrode geometry, and humidity.[41] The difference in response times for EGO- and GO-based devices may arise from the difference in band gap and the thermoelectric effect that also causes the gradual increase in dark current.

In addition to the responsivity and response time, another crucial parameter for photoconductors is the quantum efficiency (η). The quantum efficiency is defined as the number of electrons detected per incident photon, which can be estimated as, $\eta = hcR/e\lambda$, where h is the plank constant, c is the velocity of light, R is the responsivity, e is the electronic charge, and λ is the wavelength of incident light. Thus, the η values for EGO and GO are calculated as 1907 and 2.3 × 10^{-6} %, respectively, with an incident power and wavelength of UV light of 9 mW/cm^{-2} and 365 nm, respectively. The η for a few layers of reduced graphene oxide nanosheets was reported to be 1274%.[18] The large difference in the responsivity and quantum efficiency between EGO and GO may relate to defect states that trap the photoexcited electrons and play a role in

Table 1. Different Parameters of EGO- and GO-Based Devices

	EGO			GO		
P (mW/cm^2)	80	20	9	80	20	9
I_{ph} (μA)	8000	5000	5000	1.91 ×10^{-4}	0.55 ×10^{-4}	0.23 ×10^{-4}
R (A/W)	1	2.5	5.6	5.9 ×10^{-9}	6.8 ×10^{-9}	6.3 ×10^{-9}
τ_r (s)	16	15	10	0.60	0.40	0.30
τ_f (s)	4	5	4	0.30	0.40	0.40

https://doi.org/10.1021/acsomega.4c03882
ACS Omega 2024, 9, 32942−32948

the desorption and readsorption of oxygen moieties but not into the photocurrent.[42]

4. CONCLUSIONS

Despite many studies involving UV sensors with wide band gap materials, two-dimensional materials have appeared as the most promising material for UV sensors because of their tunable band gap, flexibility, and large surface area. To date, a few studies have reported on the detection of UV radiation with GO or RGO film-based UV sensors, where the GO was obtained from graphite. Here, we investigated the effect of UV irradiation on the conductivity of EGO on SiC and GO film on glass obtained from Hummer's oxidation of graphite. EG on SiC was prepared by high-temperature (∼1350 °C) annealing of SiC in a UHV chamber. Then, the EG on SiC was oxidized by a soft drop-cast procedure using Hummer's oxidizing agent, which resulted in one to three layers of graphene oxide supported on the SiC substrate. Following the characterization of EGO and GO by Raman and XPS, the devices were made by placing two copper electrodes in parallel onto the graphene oxide layers. The effect of UV light on the conductivity of the devices was measured by real-time current measurements between two copper electrodes upon the intermittent irradiation of the UV light. The positive response of the UV light was realized by the increased current (Ids) upon irradiation of UV light, which returned to its original value while the UV source is turned OFF. With a channel distance of 2 mm and UV power of 80 mW/cm^2, the photocurrent (I_{ph}) for EGO on SiC was 8 mA, which linearly changes with UV power. In the case of GO on glass, the I_{ph}value is 0.2 nA with a similar setup. The photoresponse and falling time for EGO on SiC (∼16 and ∼4 s) are much higher than those of the GO film (0.6 and 0.3 s). The photoresponsivities for EGO and GO at a power of 9 mW/cm^2 are 5.6 and 6.3 × 10^{-9} A/W, respectively. The estimated quantum efficiency for EGO on SiC is 1907%. It is expected that both the photocurrent and responsivity of EGO on SiC can be magnified by improving the device consisting of an array of microelectrodes. Because of the advantages of the EG on SiC concerning the stability and wafer scale growth, the present study is expected to lead the development of lab-on-chip-based ultrasensitive UV sensors.

■ ASSOCIATED CONTENT

Supporting Information

The Supporting Information is available free of charge at https://pubs.acs.org/doi/10.1021/acsomega.4c03882.

Real-time Ids values for GO thin film on SiC (Figure S1a), as-purchased SiC, pristine epitaxial graphene on SiC, and epitaxial graphene oxide (EGO) on SiC with channel length (distance between two Cu electrodes) of 2 and 8 mm (Figure S1b) upon periodic irradiation of UV light; estimation of response and falling times from real-time Ids values for EGO and GO-based device upon irradiation of UV for one cycle; a typical scanning tunneling microscopy (STM) image of oxidized epitaxial graphene (EG) on SiC that reflects the one to three layers of EGO onto the SiC substrate (PDF)

■ AUTHOR INFORMATION

Corresponding Author

Md. Zakir Hossain − *Gunma University Initiative for Advanced Research (GIAR), Gunma University, Kiryu 376-0023, Japan;* orcid.org/0000-0002-8193-3018; Email: zakir@gunma-u.ac.jp

Author

Ogawa Kosei − *Department of Chemistry and Molecular Biology, Gunma University, Kiryu 376-8515, Japan*

Complete contact information is available at: https://pubs.acs.org/10.1021/acsomega.4c03882

Author Contributions

Conceptualization, methodology, reviewing, and editing: M.Z.H.; data acquisition and writing the first draft preparation: O.K.

Funding

The authors thank GIAR, Gunma University for funding this work.

Notes

The authors declare no competing financial interest.

■ ACKNOWLEDGMENTS

Thanks to Professor Ozaki of Gunma University for generously allowing Raman spectroscopy measurement.

■ REFERENCES

(1) *Ultraviolet light and its uses, by Dabid Cycleback*, 2018, Bookboon, The eBook Company.

(2) Duarte, I. A. G.; Hafner, M. F. S.; Malvestiti, A. A. Ultraviolet radiation emitted by lamps, TVs, tablets and computers: are there risks for the population? *An Bras Dermatol.* **2015**, *90*, 595−597.

(3) Monroy, E.; Omn s, F.; Calle, F. Wide-bandgap semiconductor ultraviolet photodetectors. *Semicond. Sci. Technol.* **2003**, *18*, R33.

(4) Razeghi, M.; Rogalski, A. Semiconductor ultraviolet detectors. *Appl. Phys.* **1996**, *12*, 7433−7473.

(5) Watson, M.; Holman, D. M.; Maguire-Eisen, M. Ultraviolet radiation exposure and its impact on skin cancer risk. *Semin. Oncol. Nurs.* **2016**, *32*, 241−254.

(6) D'Orazio, J.; Jarrett, S.; Amaro-Ortiz, A.; Scott, T. UV radiation and the skin. *Int. J. Mol. Sci.* **2013**, *14*, 12222−12248.

(7) Gedamu, D.; Paulowicz, I.; Kaps, S.; Lupan, O.; Wille, S.; Haidarschin, G.; Mishra, Y. K.; Adelung, R. Rapid fabrication technique for interpenetrated ZnO nanotetrapod networks for fast uv sensors. *Adv. Mater.* **2014**, *26*, 1541−1550.

(8) Fang, X.; Bando, Y.; Liao, M.; Gautam, U. K.; Zhi, C.; Dierre, B.; Liu, B.; Zhai, T.; Sekiguchi, T.; Koide, Y.; Golberg, D. Single-crystalline ZnS nanobelts as ultraviolet-light sensors. *Advance Materials* **2009**, *21*, 2034−2039.

(9) Wang, X.; Zhang, Y.; Chen, X.; He, M.; Liu, C.; Yin, Y.; Zou, X.; Li, S. Ultrafast, superhigh gain visible-blind UV detector and optical logic gates based on nonpolar a-axial GaN nanowire. *Nanoscale* **2014**, *6*, 12009−12017.

(10) Lou, Z.; Li, L.; Shen, G. Ultraviolet/visible photodetectors with ultrafast, high photosensitivity based on 1D ZnS/CdS heterostructures. *Nanoscale* **2016**, *8*, 5219−5225.

(11) Fu, X. Q.; Wang, C.; Feng, P.; Wang, T. H. Anomalous photoconductivity of CeO_2 nanowires in air. *Appl. Phys. Lett.* **2007**, *91*, No. 073104.

(12) Choi, W.; Cho, M. Y.; Konar, A.; Lee, J. H.; Cha, G.-B.; Hong, S. C.; Kim, S.; Kim, J.; Jena, D.; Joo, J.; et al. High-detectivity multilayer MoS_2 phototransistors with spectral response from ultraviolet to infrared. *Adv. Mater.* **2012**, *24*, 5832−5836.

(13) Lupan, O.; Schütt, F.; Postica, V.; Smazna, D.; Mishra, Y. K.; Adelung, R. Sensing performances of pure and hybridized carbon nanotubes-ZnO nanowire networks: A detailed study. *Sci. Rep.* **2017**, *7*, 14715.

(14) Nunes, D.; Pimentel, A.; Araujo, A.; Calmeiro, T. R.; Panigrahi, S.; Pinto, J. V.; Barquinha, P.; Gama, M.; Fortunato, E.; Martins, R.

Enhanced uv flexible photodetectors and photocatalysts based on tio2 nanoplatforms. *Top Catal.* **2018**, *61*, 1591−1606.
(15) Nasiri, N.; Bo, R.; Wang, F.; Fu, L.; Tricoli, A. Ultraporous electron-depleted ZnO nanoparticle networks for highly sensitive portable visible-blind UV photodetectors. *Adv. Mater.* **2015**, *27*, 4336−4343.
(16) Mueller, T.; Xia, F.; Avouris, P. Graphene photodetectors for high-speed optical communications. *Nat. Photonics* **2010**, *4*, 297−301.
(17) Chitara, B.; Krupanidhi, S. B.; Rao, C. N. R. Solution processed reduced graphene oxide ultraviolet detector. *Appl. Phys. Lett.* **2011**, *99*, 113114.
(18) Shelke, N. T.; Karche, B. R. Ultraviolet photosensor based on few-layered reduced graphene oxide nanosheets. *Appl. Surf. Sci.* **2017**, *418*, 374−379.
(19) Novoselov, K. S.; Geim, A. K.; Morozov, S. V.; Jiang, D.; Zhang, Y.; Dubonos, S. V.; Grigorieva, I. V.; Firsov, A. A. Electric field effect in atomically thin carbon films. *Science* **2004**, *306*, 666−669.
(20) Geim, A. K.; Novoselov, K. S.The rise of graphene. In *Nanoscience and Technology*; Co-Published with Macmillan Publishers Ltd: UK, 2009; pp 11−19 ISBN 978−981−4282−68−0.
(21) Backes, C.; Abdelkader, A. M.; Alonso, C.; Andrieux-Ledier, A.; Arenal, R.; Azpeitia, J.; Balakrishnan, N.; Banszerus, L.; Barjon, J.; Bartali, R.; et al. Production and processing of graphene and related materials. *2D Mater.* **2020**, *7*, No. 022001.
(22) Sun, J.; Liu, Y. Unique constant phase element behavior of the electrolyte−graphene interface. *Nanomaterials* **2019**, *9*, 923.
(23) Du, X.; Guo, P.; Song, H.; Chen, X. Graphene nanosheets as electrode material for electric double-layer capacitors. *Electrochim. Acta* **2010**, *55*, 4812−4819.
(24) Shahdeo, D.; Roberts, A.; Abbineni, N.; Gandhi, S. Graphene based sensors. *Comprehensive Anal. Chem.* **2020**, *91*, 175−199.
(25) Nair, R. R.; Blake, P.; Grigorenko, A. N.; Novoselov, K. S.; Booth, T. J.; Stauber, T.; Peres, N. M. R.; Geim, A. K. Fine structure constant defines visual transparency of graphene. *Science* **2008**, *320*, 1308.
(26) Ito, J.; Nakamura, J.; Natori, A. Semiconducting nature of the oxygen-adsorbed graphene sheet. *J. Appl. Phys.* **2008**, *103*, 113712−113716.
(27) Hossain, M. Z.; Razak, M. B. A.; Yoshimoto, S.; Mukai, K.; Koitaya, T.; Yoshinobu, J.; Sone, H.; Hosaka, S.; Hersam, M. C. Aqueous-phase oxidation of epitaxial graphene on the silicon face of SiC(0001). *J. Phys. Chem. C* **2014**, *118*, 1014−1020.
(28) Nourbakhsh, A.; Cantoro, M.; Vosch, T.; Pourtois, G.; Clemente, F.; van der Veen, M. H.; Hofkens, J.; Heyns, M. M.; De Gendt, S.; Sels, B. F. Bandgap opening in oxygen plasma-treated graphene. *Nanotechnology* **2010**, *21*, No. 435203.
(29) Huang, H.; Li, Z.; She, J.; Wang, W. Oxygen density dependent band gap of reduced graphene oxide. *J. Appl. Phys.* **2012**, *111*, 054317−054320.
(30) Chang, H. X.; Sun, Z. H.; Yuan, Q. H.; Ding, F.; Tao, X. M.; Yan, F.; Zheng, Z. J. Thin film field-effect phototransistors from bandgap-tunable solution-processed, few-layer reduced graphene oxide films. *Adv. Mater.* **2010**, *22*, 4872−4876.
(31) Wang, Z.; Zhan, X.; Wang, Y.; Muhammad, S.; Huang, Y.; He, J. A flexible UV nanosensor based on reduced graphene oxide decorated ZnO nanostructures. *Nanoscale* **2012**, *4*, 2678−2684.
(32) Chitara, B.; Panchakarla, L.; Krupanidhi, S.; Rao, C. N. R. Infrared photodetectors based on reduced graphene oxide and graphene nanoribbons. *Adv. Mater.* **2011**, *23*, 5419−5424.
(33) Abusultan, A.; Abunahla, H.; Halawani, Y.; Mohammad, B.; Alamoodi, N.; Alazzam, A. Artificial intelligence-aided low cost and flexible graphene oxide-based paper sensor for ultraviolet and sunlight monitoring. *Nanoscale Res. Lett.* **2022**, *17*, 89.
(34) Hummers, W. S.; Offeman, R. E. Preparation of graphitic oxide. *J. Am. Chem. Soc.* **1958**, *80*, 1339.
(35) Van Bommel, A. J.; Crombeen, J. E.; Van Tooren, A. LEED and Auger electron observations of the SiC(0001) surface. *Surf. Sci.* **1975**, *48*, 463.
(36) Zou, Y.; Zhang, Y.; Hu, Y.; Gu, H. Ultraviolet detector based on wide bandgap semiconductor nanowaire: A review. *Sensor* **2018**, *18*, 2072.
(37) Zhou, H.; Yu, W. J.; Liu, L.; Cheng, R.; Chen, Y.; Huang, X.; Liu, Y.; Wang, Y.; Huang, Y.; Duan, X. Chemical vapour deposition growth of large single crystals of monolayer and bilayer graphene. *Nat. Commun.* **2013**, *4*, 2096.
(38) Abid; Sehrawat, P.; Islam, S. S.; Mishra, P.; Ahmad, S. Reduced graphene oxide (rGO) based wideband optical sensor and the role of Temperature, Defect States and Quantum Efficiency. *Sci. Rep* **2018**, *8*, 3537.
(39) Chang, H.; Sun, Z.; Saito, M.; Yuan, Q.; Zhang, H.; Li, J.; Wang, Z.; Fujita, T.; Ding, F.; Zheng, Z.; Yan, F.; Wu, H.; Chen, M.; Ikuhara, Y. Regulating Infrared Photoresponses in Reduced Graphene Oxide Phototransistors by Defect and Atomic Structure Control. *ACS Nano* **2013**, *7*, 6310−6320.
(40) Chitara, B.; Krupanidhi, S. B.; Rao, C. N. R. Solution processed reduced graphene oxide ultraviolet detector. *Appl. Phys. Lett.* **2011**, *99*, 113114−113116.
(41) Zhang, X.; Li, R.; Yu, Y.; Dai, F.; Jiang, R.; Guo, J.; Hu, W.; Ni, Z.; Lu, J. Dark Current mechanism and suppression strategies for infrared photodetectors based on two-dimensional materials. *Laser Photonics Rev.* **2024**, *18*, No. 2300936.
(42) Aldalbahi, A.; Li, E.; Rivera, M.; Velazquez, R.; Altalhi, T.; Peng, X.; Feng, P. X. A new approach for fabrications of SiC based photodetectors. *Sci. Rep.* **2016**, *6*, No. 23457.

https://doi.org/10.1021/acsomega.4c03882
ACS Omega 2024, 9, 32942−32948